The influence of design parameters on the performance of FBAR in 10–14 GHz

*N.I.M.*Nor[1,*], *R.A.M.* Osman[1], *M.S.* Idris[2], *N.* Khalid[1], *M.* Mohamad Isa[1], *N.* Ahmad[1], *Siti S.* Mat Isa[1], *Muhammad M.* Ramli[1], and *S.R.* Kasjoo[1]

[1]School of Microelectronic Engineering, Universiti Malaysia Perlis, Pauh Putra Campus 02600 Arau, Perlis, Malaysia
[2]School of Material Engineering, Universiti Malaysia Perlis, Jejawi Campus 02600 Arau, Perlis, Malaysia

Abstract. This research presents the analysis of the influence of design parameters on the performance of film bilk acoustic wave resonator (FBAR) working from 10 GHz to 14 GHz. The analysis is done by implementing one-dimensional (1-D) modellings, which are 1-D Mason model and Butterworth Van Dyke (BVD) model. The physical parameters such as piezoelectric materials and its thickness, and size of area affecting the characteristics of the FBAR are analyzed in detail. Zinc oxide (ZnO) and aluminum nitride (AlN) are chosen as the piezoelectric materials. The resonance area is varied at 25μm×25μm to 35μm×35μm. From the analysis, it is found that as the frequency increases, the thickness of the piezoelectric material decreases. Meanwhile, the static capacitance increases as the frequency increases. It is also found that as the area increases, the electrical impedance and static capacitance also increases.

1 Introduction

High demand for wireless communications technology and video has led to demand for more channels and wider bandwidth. Conventional frequency bands (below 6 GHz) are too congested. Therefore, to meet this demand, the study on the receiving system that works at frequency higher than 10 GHz has increased. Film bulk acoustic wave resonator (FBAR) filters and FBAR diplexers designed using microelectromechanical system (MEMS) technology have been widely used for WiFi and WiMAX applications. Such MEMS components have shown better performance and a higher integration level, and the same performance is expected to be achieved in Ku-band transceivers by using FBAR filters. FBARs operating in the frequency range of 5 GHz to 20 GHz have been reported to show a very high quality (Q) factor, good power handling and small size. The most common piezoelectric materials used for development of FBAR are aluminum nitride (AlN) and zinc oxide (ZnO) [1-4]. FBARs based on lead zirconate titanate (PZT) and cadmium sulphide (CdS) are also found in the literature [5-6]. CdS has low acoustic impedance and an electromechanical coupling coefficient (~2.4%). PZT has good performance in terms of the electromechanical coupling coefficient (k^2_{eff}) values of 19.8%, but has high intrinsic losses at high frequencies [1]. Thus, PZT is mostly used for low-frequency FBAR devices or applications that do not require a high Q factor [7]. For higher frequency applications, ZnO and AlN are the most suitable piezoelectric materials. These materials have the same hexagonal wurtzite structure. Although the coupling coefficient of ZnO is higher than AlN, AlN is superior to ZnO due to its moderate mechanical coupling factor, higher acoustic velocity and higher Q value. This makes AlN suitable to fabricate bulk acoustic wave (BAW) resonators/filters in several gigahertzes (GHz). Furthermore, AlN is compatible with CMOS technology and more easily manufactured compared to ZnO [7-8].

Modelling is a fundamental step in analyzing the performance of an FBAR. Several 1-D models have been proposed in order to characterize the electrical behavior of the FBAR. The 1-D Mason model is mainly used to represent the electrical behavior of BAW resonators and has been widely employed in work related to it [9-10]. The Krimholtz-Leedom-Matthaei (KLM) and Butterworth Van Dyke (BVD) model also provide a very good approach for characterizing the electrical behavior of the FBAR at fundamental modes and higher harmonics [11-12]. Therefore, in this work, the both models are implemented in the simulation in order to characterize the performance of the FBAR.

2 Design and Modelling of FBAR

2.1 FBAR Concept

FBAR is one of the technologies for fabricating BAW devices, the first FBAR device being released by Lakin and Wang in 1981. Figure 1 shows the acoustic wave propagation in FBAR through its active layer structure, which is usually a piezoelectric material. The acoustic

* Corresponding author: izza@unimap.edu.my

wave causes the deformation of the piezoelectric material. Therefore, the actuation and detection mechanisms involved in FBAR operation are due to the piezoelectric and inverse piezoelectric effects. By using these principles, a voltage applied to the resonators electrodes induces strain of the acoustic layer, and vice versa, and following a mechanical strain of the acoustic layer a voltage can be read out of the electrodes [13].

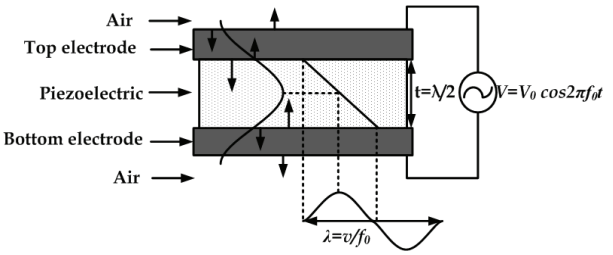

Fig. 1. Bulk Acoustic Wave Propagation in FBAR [13].

The resonance frequency of an FBAR operating in fundamental, longitudinal mode is determined mainly by the thickness (t) of the piezoelectric layer given as:

$$\theta = \frac{2\pi f_0 t}{v^D} \tag{1}$$

where θ is the phase, v^D is acoustic velocity, f is the frequency of acoustic wave propagating through the bulk acoustic layer and t is the thickness of the piezoelectric film. The acoustic velocity can be calculated using the approximation given as :

$$v^D = \sqrt{\frac{c_{33}^D}{\rho}} \tag{2}$$

where c^D_{33} is the elastic stiffness at constant electric displacement and ρ is the density of the piezoelectric material.

At resonance ($f=f_0$), the acoustic phase of the film is $\theta=\pi$, under these conditions, the f_0 can be calculated as in [13]:

$$f_0 = \frac{v_L}{2t} \tag{3}$$

From Equation 3, it follows that resonance occurs when the film thickness is equal to half the wavelength of the acoustic wave. As shown in Fig. 1, the acoustic wave is confined by the reflecting electrode surfaces at the thin film interface where t must be half the acoustic wavelength, ignoring the electrode loading effects.

2.1 1-D Mason Model

The Mason model has been widely used in deriving solutions for the wave propagation through the acoustic layer by using the network theory approach. Fig. 2 shows the thickness excitation of the piezoelectric layer, ignoring the electrodes. The piezoelectric layer can be seen as a three-port component. Two ports are the mechanical ports presented by the forces (F) and the displacement velocity (v). The other port is the electrical port given by voltage (V) and current (I).

The electrical input impedance of a single piezoelectric layer is given as:

$$Z_{in} = \frac{1}{jwC}\left(1 - k_t^2 \frac{\tan(kd/2)}{kd/2}\right) \tag{4}$$

where d is the thickness of the piezoelectric layer. F_1 and F_2 are the forces on the top and bottom surface of the resonator, respectively. v_1 and v_2 represent the acoustic velocities of the top and bottom surface plane of the resonator, respectively. V is the external electric voltage and I is the current. C is the static capacitance, $\omega=2\pi f$ is the angular frequency, $k = \omega\ v_L$ where v_L is the longitudinal acoustic wave velocity and $h=e/\varepsilon_s$ where e is piezoelectric coefficient and ε_s is the permittivity of the piezoelectric layer. k_t^2 can be computed using equation 2; while C_0 is given in equation 6 where A is the area.

$$k_t^2 = \frac{e_{33}^2}{c_{33}^D \varepsilon_{33}^s} \tag{5}$$

$$C_o = \frac{\varepsilon A}{d} \tag{6}$$

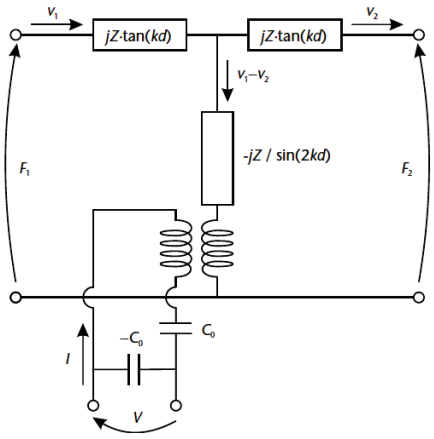

Fig. 2. Three-Port Mason"s Model Equivalent Circuit [7]

2.2 BVD Model

The Mason model may be simplified to the six-lumped element model under the assumption that FBARs have very thin electrodes. The Butterworth- Van Dyke (BVD) model is a common lumped element equivalent circuit model used by the crystal filter to simplify the transcendental functions that totally characterize the resonators used as filter elements. This BVD model, as shown in Fig. 3 (a), comprises of a series motional inductor (L_m), motional capacitor (C_m) and motional resistor (R_m) resonator in parallel with static capacitance (C_o). The C_o is the electrical capacitance between the two electrodes through which the electric fields are

applied. The motional components (C_m, L_m and R_m) represent the electromechanical response of a piezoelectric material. BVD model is the most convenient model to use but if the loss from the electrodes is to be considered then the modified Butterworth Van Dyke Circuit (MBVD) as shown in Fig. 3 (b) is adopted instead. The MBVD includes the dielectric loss (R_o) of the piezoelectric material and electrical losses (R_s) of the electrodes [14]. This model provides a better method, both simple and accurate, for characterizing electrical behavior of the FBAR at fundamental modes and higher harmonics and designing bandpass filters [11-14].

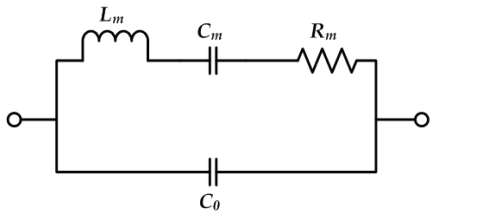

(a) BVD equivalent circuit

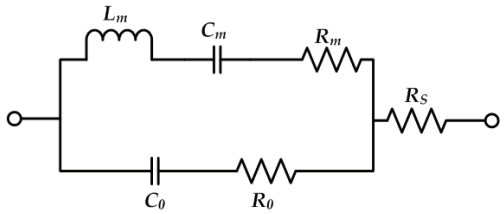

(b) MBVD equivalent circuit

Fig. 3. Equivalent Circuit for Acoustic Resonator

Several methods can be found in the literature to calculate the Q factor, for example, calculations based on the BVD) model or evaluation from the phase angle (imaginary part) of the electrical impedance given as:

$$Q_{s/p} = \frac{f_{s/p}}{2}\left[\frac{d\angle Z_{in}}{df}\right]_{f_s/f_p} \quad (7)$$

where f_s and f_p are the resonance frequencies and Z_{in} is the electrical impedance of the FBAR.

3 Results and Discussions

3.1 Influence of Different Piezoelectric Materials

In this 1-D modelling, the effect of electrodes on f_s and f_p is ignored. By referring to the estimation given in [7] for the purpose of this analysis, the bottom and top electrodes, Ru is set to 50 nm. Fig. 4 shows the relationship between resonance frequency and piezoelectric thickness. The simulation result indicates that as the thickness of the AlN and ZnO increases, the series resonance frequency decreases. This suggests that a thicker piezoelectric film reduces the influence of the electrode thickness upon the resonance frequency. This occurrence is supported by the notion that the acoustic path is proportional to the piezoelectric film thickness as modelled in equation 4. The piezoelectric film thickness is directly proportional to the acoustic path and inversely proportional to the resonance frequency. As seen from the graph too, the thickness of AlN is thicker than ZnO at the same working frequency. For example, FBAR working at 10 GHz, the thickness of AlN required is 0.553µm. Meanwhile, the thickness of ZnO is 0.318µm. This is due higher acoustic velocity of AlN which is 11050 m/s compared to ZnO that has 6350 m/s. This is true as given in equation 3.

Fig. 5 shows the relationship between different piezoelectric materials and their thicknesses on static capacitance, C_0. The results show as the frequency increases, the static capacitance gradually increases too for both AlN and ZnO. This can be verified by using equation (6), where the static capacitance is inversely proportional to the thickness of the piezoelectric material.

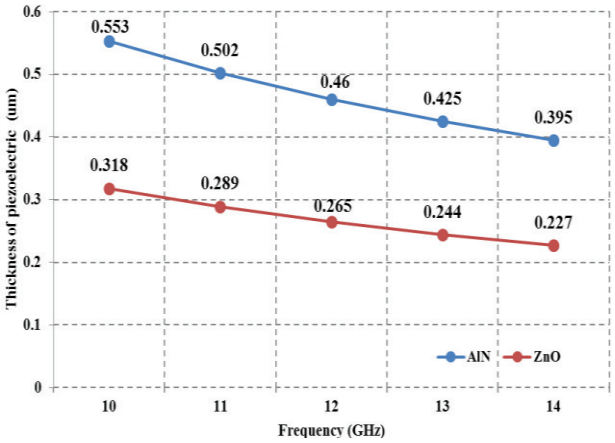

Fig. 4. Influence of Different Piezoelectric Materials and Thickness on Frequency

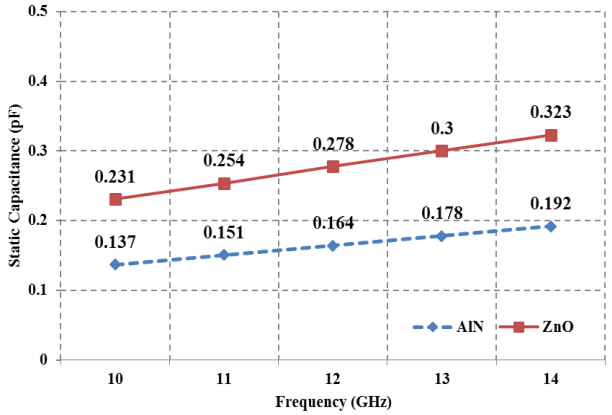

Fig. 5. Influence of Different Piezoelectric Materials

3.2 Influence of Different Area Size

Table 1 and Table 2 summarizes the influence of the resonance area on the electrical impedance, Z_{in} of FBAR using AlN and ZnO respectively. The area is set to 25x25 µm^2, 30x30 µm^2 and 35x35 µm^2 for each frequency. It is observed that as the resonance area increases, there is no significant change in the resonance frequencies, f_s and f_p. However the electrical impedance

of the FBAR decreases as the resonance area increases. According to equation 4, this is true as the electrical impedance is inversely proportional to resonance frequency.

Table 1. Influence of Area Size on Impedance, Z_{in} using AlN.

Frequency (GHz)	Area (μm^2)	f_s (GHz)	f_p (GHz)	Z_{in} (Ω)
10	25x25	09.712	09.984	0.374
	30x30	09.700	09.980	0.259
	35x35	09.710	09.980	0.191
11	25x25	10.704	11.000	1.801
	30x30	10.700	11.000	1.252
	35x35	10.700	11.000	0.923
12	25x25	11.680	12.000	0.772
	30x30	11.700	12.000	0.536
	35x35	11.700	12.000	0.393
13	25x25	12.640	12.992	0.062
	30x30	12.700	13.000	0.043
	35x35	12.600	13.000	0.032
14	25x25	13.600	13.976	0.191
	30x30	13.600	14.000	0.132
	35x35	13.600	14.000	0.097

Table 2. Influence of Area Size on Impedance, Z_{in} using ZnO.

Frequency (GHz)	Area (μm^2)	f_s (GHz)	f_p (GHz)	Z_{in} (Ω)
10	25x25	9.620	9.980	1.009
	30x30	9.630	9.990	0.765
	35x35	9.640	10.000	0.560
11	25x25	10.600	11.000	0.483
	30x30	10.600	11.000	0.304
	35x35	10.600	11.000	0.224
12	25x25	11.500	12.000	0.253
	30x30	11.600	12.000	0.175
	35x35	11.600	12.000	0.129
13	25x25	12.500	13.000	0.492
	30x30	12.500	13.000	0.343
	35x35	12.500	13.000	0.251
14	25x25	13.500	14.000	0.036
	30x30	13.500	14.000	0.025
	35x35	13.500	14.000	0.019

Fig. 6 and Fig. 7 shows the influence of different area size on the static capacitance of FBAR using AlN and ZnO respectively. From the graphs, it is clear that value of static capacitance is proportional to the size of area for both materials. Therefore, as the area size increases, the static capacitance increases too. This is verified by using equation 6. As seen from the graphs too, it is found that the values of static capacitance is higher for FBAR using ZnO compared to FBAR using AlN at the same working frequency. This is due to the permittivity value of ZnO is slightly lower than AlN. The permittivity of AlN and ZnO is 9.5 and 9.2 respectively.

From the analysis in section 3.1 and 3.2, the finding shows that the resonance frequency of FBARs is determined by the thickness and phase velocity of the piezoelectric layer. Therefore, for FBARs operating at frequencies higher than 10 GHz, the thickness of the piezoelectric layer is in the hundred nanometre (nm) scale. Furthermore, the properties and thickness of the piezoelectric materials have a significant influence on the performance of the FBAR in terms of resonance frequency, static capacitance and the electrical impedance of the FBAR.

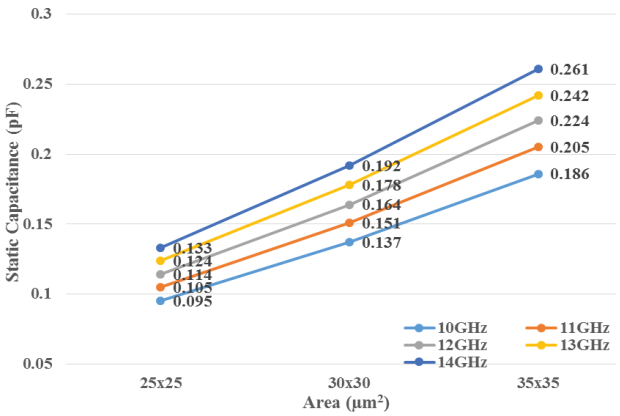

Fig. 6. Influence of Different Piezoelectric Materials

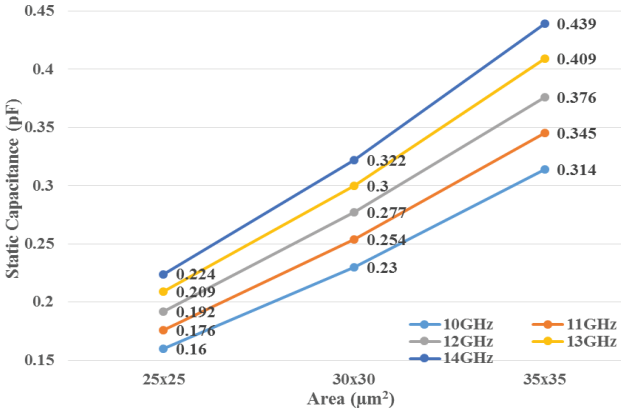

Fig. 7. Influence of Different Piezoelectric Materials

4 Conclusion

This work presented the design and analysis of FBAR using 1-D modelling. The influence of various geometrical parameters on FBAR performance were analysed and explored to find suitable solutions for designing FBAR operates at frequency higher than 10 GHz with a high Q factor and wide bandwidth. However, the presence of spurious modes at the frequency of interest due to lateral waves cannot be predicted by 1-D modelling, therefore, the three-dimensional (3-D) simulation tool will be beneficial in future work.

References

1. Klee, C. Metzmacher, et al, Materials Chemistry and Physics, **79**, pp. 143-146 (2003).

2. W.-K. Liu, K.-W. Tay, S.-C. Kuo, et al, Science in China Series G: Physics Mechanics and Astronomy, **52**, pp. 226-232 (2009).
3. R. Kubo, H. Fujii, H. Kawamura, et al, IEEE Symposium on Ultrasonics, **1**, pp. 166-169 (2003).
4. Q. X. Su, P. Kirby, E. Komuro, et al, IEEE Transactions on Microwave Theory and Techniques, **49**, pp. 769-778 (2001).
5. E. K. Kim, T. Y. Lee, Y. H. Jeong, et al, Thin Solid Films, **496**, pp. 653-657 (2006).
6. J. G. Gualtieri, J. A. Kosinski, and A. Ballato, IEEE Transactions on Ultrasonics, Ferroelectrics and Frequency Control, **41**, pp. 53-59 (1994).
7. K.-y. Hashimoto, *RF Bulk Acoustic Wave Filters for Communications,* Artech House (2009).
8. R. LANZ*, Piezoelectric Thin Films for Bulk Acoustic Wave Resonator Applications: From Processing to Microwave Filters,PhD*, ÉCOLE POLYTECHNIQUE FÉDÉRALE DE LAUSANNE (2004).
9. J. V. Tirado, *Bulk Acoustic Wave Resonators and Their Application to Microwave Devices*, PhD, Universitat Antonoma de Barcelona, (2010).
10. D. S. Shim and D. A. Feld, Int. J. RF Microw. Comput.-Aided Eng., **21**, pp. 486-495 (2011).
11. K. M. Lakin, IEEE Transactions on Ultrasonics, Ferroelectrics and Frequency Control*,* **52**, pp. 707-716, (2005).
12. H. Jin, S. R. Dong, J. K. Luo, et al., Electro. Let., **47**, pp. 424-426, (2011).
13. H. Campanella, *Acoustic Wave and Electromechanical Resonators*: Artech House (2010).
14. J. D. Larson, III, P. D. Bradley, S. Wartenberg*, et al.*, IEEE Ultrasonics Symposium, pp. 863-868, (2000).
15. M. Hara, T. Yokoyama, M. Ueda*, et al*., IEEE Ultrasonics Symposium, pp. 1152-1155, (2007).